

Demonstration of a quantum SWITCH in a Sagnac configuration

Teodor Strömberg,^{1,2,*} Peter Schiаны,^{1,2} Robert W. Peterson,² Marco Túlio Quintino,^{3,4,5} and Philip Walther^{2,†}

¹University of Vienna, Faculty of Physics & Vienna Doctoral School in Physics, Boltzmannngasse 5, A-1090 Vienna, Austria

²University of Vienna, Faculty of Physics & Research Network Quantum Aspects of Space Time (TURIS), Boltzmannngasse 5, 1090 Vienna, Austria

³Sorbonne Université, CNRS, LIP6, F-75005 Paris, France

⁴University of Vienna, Faculty of Physics, Boltzmannngasse 5, 1090 Vienna, Austria

⁵Institute for Quantum Optics and Quantum Information, Boltzmannngasse 3, 1090 Vienna, Austria

(Dated: November 24, 2022)

The quantum SWITCH is an example of a process with an indefinite causal structure, and has attracted attention for its ability to outperform causally ordered computations within the quantum circuit model. To date, realisations of the quantum SWITCH have relied on optical interferometers susceptible to minute path length fluctuations, complicating their design, limiting their performance and posing an obstacle to extending the quantum SWITCH to multiple parties. In this Letter we overcome these limitations by demonstrating an intrinsically stable quantum SWITCH utilizing a common-path geometry facilitated by a novel reciprocal and universal SU(2) polarization gadget. We certify our design by successfully performing a channel discrimination task with near unity success probability.

I. INTRODUCTION

Quantum information processing tasks are most commonly described within the framework of the quantum circuit model. In this framework an initial state gradually evolves by passing through a fixed sequence of gates. This, however, is not the most general model of computation that quantum mechanics admits, and in [1] a process that effects a superposition of quantum circuits was proposed. This process, known as the quantum SWITCH, has attracted significant theoretical [2–5] and experimental [6–13] interest. Together with the so-called Oreshkov-Costa-Brukner (OCB) process [14] it was the first example of a quantum process without a definite causal structure, and motivated the study of more general causal structures within quantum mechanics that could help bridge the gap between general relativity and quantum mechanics. The quantum SWITCH is also of practical interest, since it has been shown to allow for a computational advantage over standard quantum circuits [15, 16], an advantage which has also been demonstrated experimentally [17].

In its simplest form, the quantum SWITCH is a map that acts on two gates, U and V , and transforms them into a controlled superposition of the gates being applied in two different orders:

$$(U, V) \rightarrow UV \otimes |0\rangle\langle 0|_C + VU \otimes |1\rangle\langle 1|_C. \quad (1)$$

To date, all experimental realisations of the quantum SWITCH have been done using single photons as the physical system encoding the input and output state of the process. These implementations typically rely on folded Mach-Zehnder interferometers and polarization

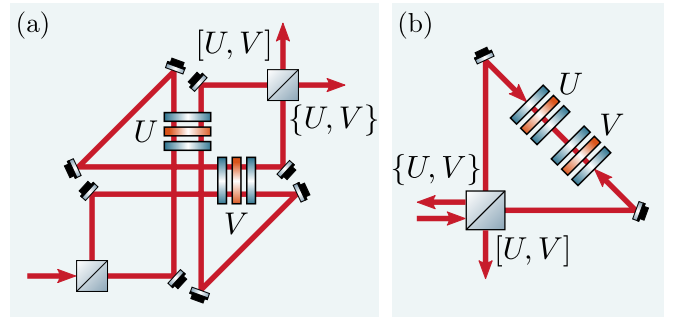


Figure 1. Path-polarization quantum SWITCH. (a) The most common implementation of the photonic quantum SWITCH utilizes the path degree of freedom of a single photon inside a Mach-Zehnder interferometer to coherently control the order in which two polarization operations U and V are applied. In this geometry, photons in different arms of the interferometer propagate through different parts of the polarization optics. (b) An implementation based on a Sagnac interferometer is fundamentally simpler and more robust, but necessitates two different propagation directions through the polarization gadgets effecting the transformations U and V . In general the operations in the two different propagation directions are not the same, limiting the use of this geometry to special cases.

optics to couple different internal degrees of freedom of the single photons. A technical challenge associated with such implementations is that the phase of the interferometer needs to be kept constant even as different choices of U and V in (1) change the interference condition. In practice, most experimental quantum SWITCHes have relied on passive phase stability during operation, limiting not only their fidelity, but also their duty cycle due to the need to periodically reset the phase. Furthermore, the geometry of the Mach-Zehnder interferometer means that single photons in the two different arms of the interferometer interact with different parts of the polarization

* Corresponding author: teodor.stroemberg@univie.ac.at

† Corresponding author: philip.walther@univie.ac.at

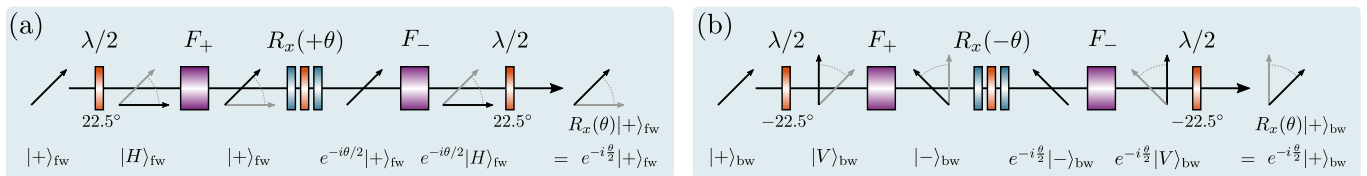


Figure 2. Reciprocal polarization gadget. The figures show the evolution of a diagonally polarized state in the two different propagation directions through a reciprocal polarization gadget implementing an R_x rotation. The arrows indicating the polarization states are drawn in the co-moving frame. Note that only differential phases between the two polarization states are indicated. **(a)** The Faraday rotators F_{\pm} rotate linear polarization by 45° , and in the forwards direction these rotations cancel the half-wave plate (HWP) rotations, indicated by $\lambda/2$. The state before the central waveplate gadget is therefore $|+\rangle$, and the correct phase gets applied. **(b)** In the backwards propagation direction the rotations of the HWP and Faraday rotators add, rotating the linear polarization by 90° . The $R_x(-\theta)$ rotation applies the desired phase to what is now the $|-\rangle$ state, which subsequently gets rotated back to $|+\rangle$, yielding the correct transformation.

optics (see Fig. 1a). The reliance on optical geometries that suffer from phase instability is necessitated by the non-reciprocity of the optical components that effect the unitary transformations U and V on the photon polarization. The works [8, 10] remedied this by using the polarization as a control degree of freedom, instead of a target, thereby enabling a common-path geometry, however this came at the expense of more cumbersome and low fidelity target qubit operations.

In this letter we overcome these limitations by designing a fully reciprocal polarization gadget capable of realising any $U \in \text{SU}(2)$, thereby enabling the use of a passively stable Sagnac geometry with perfect spatial mode overlap, while still using the polarization degree of freedom for the target qubit.

II. PHOTONIC QUANTUM SWITCH

Before describing our novel quantum SWITCH design, we will first examine the commonly used path-polarization quantum SWITCH shown in Fig. 1a. Devices of this form make use of the path degree of freedom of a single photon as a control qubit and the polarization degree of freedom of the same photon as a target qubit, meaning that the path degree of freedom is used to coherently superpose two different orders through the waveplate gadgets that act on the target qubit. These waveplate gadgets, first introduced by Simon and Mukunda, consist of two quarter-wave plates and one half-wave plate, and are capable of realising any single qubit operation [18]. If one tries to simplify the device by folding the two arms of the interferometer and creating a common path geometry, as depicted in Fig. 1b, the photon now travels through the polarization gadgets in different directions depending on the state of the control qubit. The action of a Simon-Mukunda gadget in the backwards direction is:

$$U^{\text{bw}} = PU^T P^\dagger \neq U, \quad (2)$$

where U is the unitary operation in the forwards direction, while P is a unitary operator describing the basis

change to the backwards propagation direction, the particular form of which depends on the choice of convention for the polarization states. It is possible to pick a convention such that $P = \mathbb{1}$ [19], however the residual transposition, which is a consequence of the fact that the order of the waveplates is transposed in the backwards direction, cannot be undone this way. Even in such a choice of convention, the Simon-Mukunda gadget is therefore only reciprocal for symmetric unitaires, which merely form a two parameter subset of $\text{SU}(2)$ [20].

In this work we adopt the convention $(S_1, S_2, S_3) \leftrightarrow (X, Y, Z)$ for the Stokes parameters and Pauli matrices. Written in this convention the Simon-Mukunda gadget transforms as:

$$U \rightarrow U^{\text{bw}} = ZU^T Z, \quad (3)$$

under counter propagation. Given a unitary parameterised as:

$$U = \cos \frac{\theta}{2} \mathbb{1} - i \sin \frac{\theta}{2} \vec{\sigma} \cdot \vec{n}, \quad (4)$$

where $\vec{\sigma}$ is the Pauli vector and \vec{n} the rotation axis of the unitary operation on the Bloch sphere, this transformation corresponds to:

$$[\theta \ n_x \ n_y \ n_z] \rightarrow [\theta \ -n_x \ n_y \ n_z]. \quad (5)$$

This transformation applies to any unitary operation implemented by a sequence of linear retarders under counter propagation. In addition to linear retarders, we therefore also consider circular retarders, more specifically Faraday rotators. It is a well known fact that Faraday rotators are non-reciprocal, due to the magneto-optic effect breaking Lorentz-reciprocity [21]. This property has enabled a multitude of widely adopted optical devices such as Faraday mirrors [22], optical circulators, and optical isolators [23]. Quantitatively, the non-reciprocity manifests itself as the following transformation under counter propagation:

$$[\theta \ n_y] \rightarrow [-\theta \ n_y]. \quad (6)$$

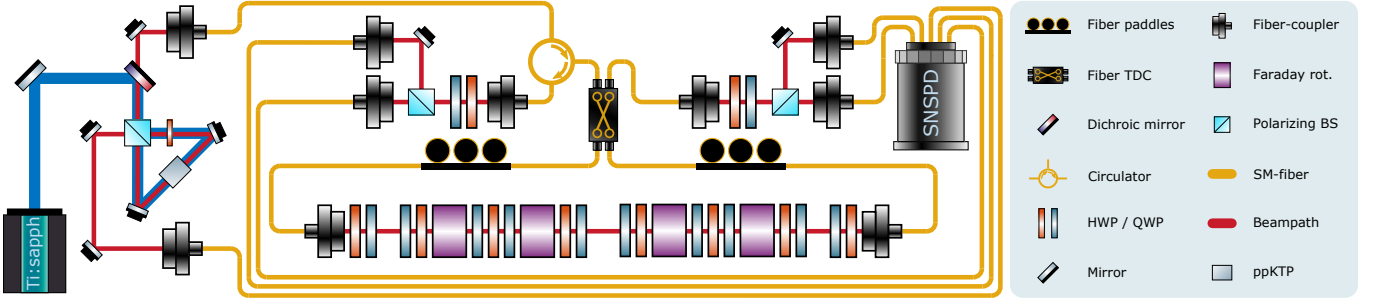


Figure 3. Experimental setup. Single photons are generated by a type-II spontaneous parametric down-conversion source using a ppKTP crystal in a collinear configuration. The signal photon is sent directly to a set of superconducting nanowire single-photon detectors (SNSPDs) to herald the presence of the idler photon. A tunable directional coupler (TDC) configured for a balanced splitting ratio sends the idler photon through a free-space path in a superposition of two propagation directions. This path contains two reciprocal polarization gadgets consisting of two Faraday rotators, four quarter-wave plates (QWPs) and three half-wave plates (HWPs) each. The two gadgets implement the unitary operators U and V . After interfering with itself on the TDC, the photon exits in one of the two TDC ports depending on whether U and V commute or anti-commute. It is then detected in one of two polarization resolving measurement stations. A fiber circulator is used to pick off photons exiting the Sagnac in the input port.

Due to the challenges of realising strong tunable magnetic fields in tabletop optics, Faraday rotators are instead packaged with permanent magnets and are usually sold with a fixed circular retardance of $\theta = \frac{\pi}{2}$, corresponding to a rotation of linear polarization by 45° . We will therefore restrict our discussion to only these Faraday rotators, and show how they can be used to construct a fully reciprocal polarization device.

III. A RECIPROCAL POLARIZATION GADGET

Since according to (5) only the X -component of the Simon-Mukunda gadget exhibits non-reciprocity, we begin by constructing a gadget capable of realising a reciprocal X -rotation:

$$G_x(\theta) = H\left(\frac{\pi}{8}\right)F_-Q\left(\frac{\pi}{2}\right)H\left(\frac{\theta + 2\pi}{4}\right)Q\left(\frac{\pi}{2}\right)F_+H\left(\frac{\pi}{8}\right). \quad (7)$$

Here H and Q refer to half- and quarter-wave plates at a given angle from the vertical axis, and F_\pm are Faraday rotators with circular retardance of $\pm\frac{\pi}{2}$. The three middle waveplates constitute a Simon-Mukunda gadget implementing a non-reciprocal X -rotation:

$$R_x(\theta + 2\pi) = -R_x(\theta) \rightarrow -R_x(-\theta). \quad (8)$$

The action of the G_x gadget in the two different propagation directions can therefore be expressed as:

$$G_x^{\text{fw}}(\theta) = -H\left(\frac{\pi}{8}\right)F_-R_x(\theta)F_+H\left(\frac{\pi}{8}\right) \quad (9)$$

$$G_x^{\text{bw}}(\theta) = -H\left(-\frac{\pi}{8}\right)F_-R_x(-\theta)F_+H\left(-\frac{\pi}{8}\right), \quad (10)$$

since for a single linear retarder at an angle φ to the vertical axis the effect of reversing the propagation direction is: $\varphi \rightarrow -\varphi$. The superscripts ‘fw’ and ‘bw’ refer

to the forwards and backwards propagation directions respectively. To see that the full gadget is reciprocal, note that:

$$H\left(\frac{\pi}{8}\right)F_- = F_+H\left(\frac{\pi}{8}\right) = -iX \quad (11)$$

$$H\left(-\frac{\pi}{8}\right)F_- = F_+H\left(-\frac{\pi}{8}\right) = -iZ, \quad (12)$$

as shown in the Appendix. The action of the gadget in the two propagation directions can therefore be simplified to:

$$G_x^{\text{fw}}(\theta) = XR_x(\theta)X = R_x(\theta) \quad (13)$$

$$G_x^{\text{bw}}(\theta) = ZR_x(-\theta)Z = R_x(\theta). \quad (14)$$

A graphical examination of the reciprocity of the gadget is shown in Fig. 2. Using this gadget as a building block, it becomes possible to construct a fully reciprocal gadget capable of implementing arbitrary unitaries:

$$G_R = Q(\theta)H(\phi)G_x(\gamma)H(-\phi)Q(-\theta). \quad (15)$$

This gadget is reciprocal due to its palindromic order, and a proof of its universality is given in the Appendix.

IV. ADVANTAGE IN A CHANNEL DISCRIMINATION TASK

To certify our that our experimental platform is capable of realising an indefinite causal order, we now present a channel discrimination task for which the quantum SWITCH strictly outperforms any causally ordered strategy. This channel discrimination problem was originally presented in Ref. [15] as a causal witness and was inspired by the task introduced in Ref. [3]. Let U_i, V_j be two qubit unitary operators belonging to the set:

$$\mathcal{G} := \left\{ \mathbb{1}, X, Y, Z, \frac{X \pm Y}{\sqrt{2}}, \frac{X \pm Z}{\sqrt{2}}, \frac{Y \pm Z}{\sqrt{2}} \right\}. \quad (16)$$

Using this set, we define two sets of pairs of operators (U_i, V_j) that either commute or anti-commute:

$$\mathcal{G}_+ := \left\{ (U_i, V_j) \mid U_i, V_j \in \mathcal{G}, U_i U_j = V_j U_i \right\} \quad (17)$$

$$\mathcal{G}_- := \left\{ (U_i, V_j) \mid U_i, V_j \in \mathcal{G}, U_i V_j = -V_j U_i \right\} \quad (18)$$

Let (U_i, V_j) be a pair of channels belonging to either \mathcal{G}_+ or \mathcal{G}_- , and consider the task of deciding to which set they belong, given only a single use of the channels. If the player has access to a quantum SWITCH, it is well known that this task can be performed deterministically. This can be seen by setting the state of the control qubit in (1) to $|+\rangle_C$ and considering the action on any target state $|\Psi\rangle_T$:

$$\begin{aligned} (UV \otimes |0\rangle\langle 0| + VU \otimes |1\rangle\langle 1|) |\Psi\rangle_T \otimes |+\rangle_C = \\ \frac{1}{2}(UV + VU) |\Psi\rangle_T \otimes |+\rangle_C + \frac{1}{2}(UV - VU) |\Psi\rangle_T \otimes |-\rangle_C. \end{aligned} \quad (19)$$

By measuring the control qubit in the $\{|+\rangle, |-\rangle\}$ basis, we can deterministically decide to which set (U_i, V_j) belongs.

For this discrimination task, the probability of successfully guessing the set can be expressed as:

$$p_s(i, j) = \begin{cases} p(|(U_i, V_j)\rangle), & \text{if } (U_i, V_j) \in \mathcal{G}_+ \\ p(-|(U_i, V_j)\rangle), & \text{if } (U_i, V_j) \in \mathcal{G}_- \end{cases} \quad (20)$$

By making use of the semidefinite programming methods presented in Ref. [24], we find that any causally ordered strategy necessarily obeys:

$$\min(p_s(i, j)) \leq 0.841. \quad (21)$$

Moreover, if the pairs of channels (U_i, U_j) are uniformly picked from \mathcal{G}_+ and \mathcal{G}_- , the average probability of correctly guessing the set with a causally ordered strategy is bounded by:

$$\frac{1}{N} \sum_{i,j} p_s(i, j) \leq \frac{90.4}{100}, \quad (22)$$

where the indices (i, j) run over all the $N = 52$ pairs of gates that commute or anti-commute. As discussed in Ref. [15], this average success probability approach can be phrased in terms of a causal non-separability witness, and in the Appendix we explicitly present such a witness. The code to certify the above values is openly available in an online repository [25].

V. EXPERIMENT

Before experimentally performing the channel discrimination task, we first show that the gadget in (15) is indeed reciprocal and universal. To this end we perform

quantum process tomography on both gadgets used in the experiment for 100 random unitaries. The resulting gate fidelities, defined as the average state fidelity under the reconstructed unitaries, are presented in the Appendix. Achieving an average gate fidelity of 0.9970 ± 0.0018 , and an average fidelity between the two propagation directions of 0.9972 ± 0.0018 , we conclude that the gadget is reciprocal and universal.

We now turn to the experimental realisation of the quantum SWITCH, pictured in Fig. 3. For the certification of the indefinite causal structure of the implemented process, we employ single photons generated using type-II spontaneous parametric down-conversion in a collinear geometry [26]. The signal photon is used as a herald for the idler photon, which is made to propagate through the quantum SWITCH. Initially a beam-splitter in the form of a tunable directional coupler (TDC) applies a Hadamard operation on the path (control) degree of freedom, thereby preparing the state:

$$|\Psi\rangle_T \otimes \frac{|0\rangle_C + |1\rangle_C}{\sqrt{2}}, \quad (23)$$

where the subscripts C and T refer to the control and target degrees of freedom respectively. The photon then passes through the polarization gadgets in a superposition of the two propagation directions, correlating the applied gate order with the control degree of freedom:

$$\begin{aligned} & \frac{1}{\sqrt{2}} UV |\Psi\rangle_T \otimes |0\rangle_C + \frac{1}{\sqrt{2}} VU |\Psi\rangle_T \otimes |1\rangle_C \\ = & \frac{1}{2} (UV + VU) |\Psi\rangle_T \otimes |+\rangle_C + \frac{1}{2} (UV - VU) |\Psi\rangle_T \otimes |-\rangle_C. \end{aligned} \quad (24)$$

Finally, the photon propagates back to the TDC which once again applies a Hadamard gate on the control qubit:

$$\frac{1}{2} \{U, V\} |\Psi\rangle_T \otimes |0\rangle_C + \frac{1}{2} [U, V] |\Psi\rangle_T \otimes |1\rangle_C. \quad (25)$$

Tracing out the target qubit and only measuring the photon's location then reveals, with unity probability, whether the gates (U, V) commute or anti-commute.

Our implementation makes use of a combination of free-space and fiber optics, which is facilitated by the intrinsic phase stability of the common-path geometry. As mentioned, the input/output beam-splitter of the Sagnac quantum SWITCH is a TDC, allowing for precise control over the splitting ratio as well as providing perfect spatial mode overlap. These two factors combine to yield a high interferometric visibility in excess of 0.9995. The two inner ports of the TDC are connected to fiber collimators that launch the photons into free space where they propagate through the two polarization gadgets in opposite directions.

A fiber-circulator is placed at the input port of the TDC to separate the backwards propagating photons from the input light. Finally, two measurement stations are used to measure the polarization of the photons in

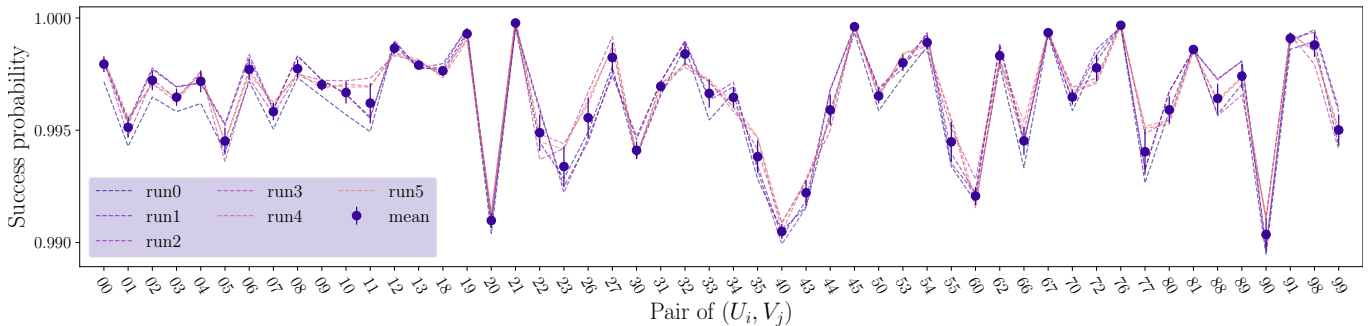


Figure 4. Success probabilities. The figure shows the success probabilities $p_s(i, j)$, which correspond to the probability for the photon to exit in the correct port of the interferometer given a pair of commuting or anti-commuting unitaries (U_i, V_j) . The six different runs of the experiment, plotted separately, exhibit high repeatability. Dashed lines show these six different experimental runs, while the solid dots indicate the mean and standard deviation taken over the same runs. The average success probability, given by the mean of value of the plot, is $\langle p_s \rangle = 0.9964$, while the highest and lowest success probabilities are $\max(p_s(i, j)) = 0.99997$ and $\min(p_s(i, j)) = 0.9895$ respectively.

either output arm of the Sagnac. The output polarization state is not directly used in witnessing the causal non-separability, as formally the target system of the quantum SWITCH is traced over. However, polarization resolving measurements allow for the polarization dependent detection efficiencies in the superconducting nanowire single-photon detectors used in the experiment to be corrected for. The fiber circulator induces a small amount of differential loss in the two interferometer outputs which is also corrected for (see Appendix).

VI. RESULTS

Each of the 52 pairs of (anti-)commuting unitary operators in the sets (17) and (18) were implemented six independent times, and for each pair of operations single-photon events were recorded for 60 seconds, giving a total measurement time of approximately 5 h, with the only downtime being the time spent rotating the waveplates. The success probabilities were then calculated separately for each run. The results of this are shown in Fig. 4. We find a minimum success probability of $\min(p_s(i, j)) = 0.9895$, and an average success probability of $\langle p_s \rangle = 0.99639 \pm 0.00007$, far exceeding the causally separable bounds of 0.841 and 0.904, respectively. Our observed average success probability can be directly compared with a non-common-path implementation of an analogous channel discrimination task presented in [6], where a success probability of 0.973 was achieved. The observed success probabilities $p_s(i, j)$ for the individual pairs of gates (U_i, V_j) additionally display a remarkably low variance, with a recorded standard deviation of $\sigma^2 = 0.0024$, demonstrating the robustness of our design. The uncertainty in the experimentally evaluated success probability is the error-propagated observed standard deviation for the constituent success probabilities $p_s(i, j)$ in the six runs.

VII. CONCLUSION AND DISCUSSION

We have demonstrated for the first time a passively stable quantum SWITCH in a Sagnac geometry, greatly simplifying the construction and operation of the device, while simultaneously increasing its fidelity, robustness and duty cycle. Our implementation is facilitated by a novel polarization gadget that combines different forms of non-reciprocity to unlock fully reciprocal and universal polarization transformations. The simplicity of our approach will aid in the construction of higher order quantum SWITCHes, which have so far not been realised due to the complexity of the associated phase stabilisation. We also anticipate that the polarization gadget presented here will have applications outside the field of indefinite causality, for example in the realisation of passively stable and tunable beam-splitters and partially polarizing beam-splitters based on common-path interferometers [27], as well as implementations of generalized measurements on polarization qubits [28].

ACKNOWLEDGMENTS

R.W.P. acknowledges support from the ESQ Discovery program (Erwin Schrödinger Center for Quantum Science and Technology), hosted by the Austrian Academy of Sciences (ÖAW). P.W. acknowledges support from the research platform TURIS, the European Commission through EPIQUS (no. 899368) and AppQInfo (no. 956071). from the Austrian Science Fund (FWF) through BeyondC (F7113) and Research Group 5 (FG5), from the AFOSR via PhoQuGraph (FA8655-20-1-7030) and QTRUST (FA9550-21-1-0355), from the John Templeton Foundation via the Quantum Information Structure of Spacetime (QISS) project (ID 61466), and from the Austrian Federal Ministry for Digital and Economic Affairs, the National Foundation for Research, Technol-

ogy and Development and the Christian Doppler Research Association.

COMPETING INTERESTS STATEMENT

The authors have no competing interests to declare.

AUTHOR CONTRIBUTIONS

All authors contributed to writing the manuscript.

DATA AVAILABILITY

All data is openly available on Zenodo under doi.org/identifier

-
- [1] G. Chiribella, G. M. D'Ariano, P. Perinotti, and B. Valiron, Quantum computations without definite causal structure, *Phys. Rev. A* **88**, 022318 (2013), [arXiv:0912.0195 \[quant-ph\]](https://arxiv.org/abs/0912.0195).
- [2] T. Colnaghi, G. M. D'Ariano, S. Facchini, and P. Perinotti, Quantum computation with programmable connections between gates, *Physics Letters A* **376**, 2940 (2012), [arXiv:1109.5987 \[quant-ph\]](https://arxiv.org/abs/1109.5987).
- [3] G. Chiribella, Perfect discrimination of no-signalling channels via quantum superposition of causal structures, *Phys. Rev. A* **86**, 040301 (2012), [arXiv:1109.5154 \[quant-ph\]](https://arxiv.org/abs/1109.5154).
- [4] A. Feix, M. Araújo, and Č. Brukner, Quantum superposition of the order of parties as a communication resource, *Phys. Rev. A* **92**, 052326 (2015), [arXiv:1508.07840 \[quant-ph\]](https://arxiv.org/abs/1508.07840).
- [5] X. Zhao, Y. Yang, and G. Chiribella, Quantum Metrology with Indefinite Causal Order, *Phys. Rev. Lett.* **124**, 190503 (2020), [arXiv:1912.02449 \[quant-ph\]](https://arxiv.org/abs/1912.02449).
- [6] L. M. Procopio, A. Moqanaki, M. Araújo, F. Costa, I. Alonso Calafell, E. G. Dowd, D. R. Hamel, L. A. Rozema, Č. Brukner, and P. Walther, Experimental superposition of orders of quantum gates, *Nature Communications* **6**, 7913 (2015), [arXiv:1412.4006 \[quant-ph\]](https://arxiv.org/abs/1412.4006).
- [7] G. Rubino, L. A. Rozema, A. Feix, M. Araújo, J. M. Zeuner, L. M. Procopio, Č. Brukner, and P. Walther, Experimental verification of an indefinite causal order, *Science Advances* **3**, e1602589 (2017), [arXiv:1608.01683 \[quant-ph\]](https://arxiv.org/abs/1608.01683).
- [8] K. Goswami, C. Giarmatzi, M. Kewming, F. Costa, C. Branciard, J. Romero, and A. G. White, Indefinite Causal Order in a Quantum Switch, *Phys. Rev. Lett.* **121**, 090503 (2018), [arXiv:1803.04302 \[quant-ph\]](https://arxiv.org/abs/1803.04302).
- [9] G. Rubino, L. A. Rozema, F. Massa, M. Araújo, M. Zych, Č. Brukner, and P. Walther, Experimental entanglement of temporal order (2017) [arXiv:1712.06884 \[quant-ph\]](https://arxiv.org/abs/1712.06884).
- [10] K. Goswami, Y. Cao, G. A. Paz-Silva, J. Romero, and A. G. White, Increasing communication capacity via superposition of order, *Physical Review Research* **2**, 033292 (2020), [arXiv:1807.07383 \[quant-ph\]](https://arxiv.org/abs/1807.07383).
- [11] G. Rubino, L. A. Rozema, D. Ebler, H. Kristjánsson, S. Salek, P. Allard Guérin, A. A. Abbott, C. Branciard, Č. Brukner, G. Chiribella, and P. Walther, Experimental quantum communication enhancement by superposing trajectories, *Physical Review Research* **3**, 013093 (2021), [arXiv:2007.05005 \[quant-ph\]](https://arxiv.org/abs/2007.05005).
- [12] Y. Guo, X.-M. Hu, Z.-B. Hou, H. Cao, J.-M. Cui, B.-H. Liu, Y.-F. Huang, C.-F. Li, G.-C. Guo, and G. Chiribella, Experimental Transmission of Quantum Information Using a Superposition of Causal Orders, *Phys. Rev. Lett.* **124**, 10.1103/PhysRevLett.124.030502 (2020), [arXiv:1811.07526 \[quant-ph\]](https://arxiv.org/abs/1811.07526).
- [13] H. Cao, J. Bavaresco, N.-N. Wang, L. A. Rozema, C. Zhang, Y.-F. Huang, B.-H. Liu, C.-F. Li, G.-C. Guo, and P. Walther, Experimental semi-device-independent certification of indefinite causal order, arXiv e-prints (2022), [arXiv:2202.05346 \[quant-ph\]](https://arxiv.org/abs/2202.05346).
- [14] O. Oreshkov, F. Costa, and Č. Brukner, Quantum correlations with no causal order, *Nature Communications* **3**, 1092 (2012), [arXiv:1105.4464 \[quant-ph\]](https://arxiv.org/abs/1105.4464).
- [15] M. Araújo, F. Costa, and Č. Brukner, Computational Advantage from Quantum-Controlled Ordering of Gates, *Phys. Rev. Lett.* **113**, 250402 (2014), [arXiv:1401.8127 \[quant-ph\]](https://arxiv.org/abs/1401.8127).
- [16] M. J. Renner and Č. Brukner, Computational advantage from a quantum superposition of qubit gate orders, *Physical Review Letters* **128**, 230503 (2022), [arXiv:2112.14541 \[quant-ph\]](https://arxiv.org/abs/2112.14541).
- [17] K. Wei, N. Tischler, S.-R. Zhao, Y.-H. Li, J. M. Arrazola, Y. Liu, W. Zhang, H. Li, L. You, Z. Wang, Y.-A. Chen, B. C. Sanders, Q. Zhang, G. J. Pryde, F. Xu, and J.-W. Pan, Experimental Quantum Switching for Exponentially Superior Quantum Communication Complexity, *Phys. Rev. Lett.* **122**, 120504 (2019), [arXiv:1810.10238 \[quant-ph\]](https://arxiv.org/abs/1810.10238).
- [18] R. Simon and N. Mukunda, Minimal three-component SU(2) gadget for polarization optics, *Physics Letters A* **143**, 165 (1990).
- [19] T. Strömberg, P. Schiainsky, M. T. Quintino, M. Antesberger, L. Rozema, I. Agresti, Č. Brukner, and P. Walther, Experimental superposition of time directions, arXiv preprint [arXiv:2211.01283](https://arxiv.org/abs/2211.01283), [arXiv:2211.01283 \[quant-ph\]](https://arxiv.org/abs/2211.01283).
- [20] P. Schiainsky, T. Strömberg, D. Trillo, V. Saggio, B. Dive, M. Navascués, and P. Walther, Experimental superposition of time directions, arXiv e-prints, [arXiv:2211.01283](https://arxiv.org/abs/2211.01283) (2022), [arXiv:2211.01283 \[quant-ph\]](https://arxiv.org/abs/2211.01283).
- [21] V. S. Asadchy, M. S. Mirmoosa, A. Diaz-Rubio, S. Fan, and S. A. Tretyakov, Tutorial on electromagnetic nonreciprocity and its origins, *Proceedings of the IEEE* **108**, 1684 (2020).
- [22] M. Martinelli, A universal compensator for polarization changes induced by birefringence on a retracing beam, *Optics Communications* **72**, 341 (1989).
- [23] B. E. Saleh and M. C. Teich, *Fundamentals of photonics* (John Wiley & sons, 2019).
- [24] J. Bavaresco, M. Muraio, and M. T. Quintino, Strict hierarchy between parallel, sequential, and indefinite-causal-

- order strategies for channel discrimination, *Phys. Rev. Lett.* **127**, 200504 (2021), 2011.08300 [quant-ph].
- [25] M. T. Quintino, <https://github.com/mtcq> (2022).
- [26] C. Greganti, P. Schiansky, I. A. Calafell, L. M. Procopio, L. A. Rozema, and P. Walther, Tuning single-photon sources for telecom multi-photon experiments, *Opt. Express* **26**, 3286 (2018).
- [27] J. Flórez, N. J. Carlson, C. H. Nacke, L. Giner, and J. S. Lundeen, A variable partially polarizing beam splitter, *Review of Scientific Instruments* **89**, 023108 (2018), arXiv:1709.05209 [physics.ins-det].
- [28] P. Kurzyński and A. Wójcik, Quantum walk as a generalized measuring device, *Physical review letters* **110**, 200404 (2013), arXiv:1208.1800 [quant-ph].

Appendix A: Supplementary material

1. Definitions and conventions

In this work we use the following convention for our polarization states:

$$\begin{aligned}
 |H\rangle &= \begin{bmatrix} 1 \\ 0 \end{bmatrix}, & |V\rangle &= \begin{bmatrix} 0 \\ 1 \end{bmatrix}, \\
 |+\rangle &= \frac{1}{\sqrt{2}} \begin{bmatrix} 1 \\ 1 \end{bmatrix}, & |-\rangle &= \frac{1}{\sqrt{2}} \begin{bmatrix} 1 \\ -1 \end{bmatrix}, \\
 |L\rangle &= \frac{1}{\sqrt{2}} \begin{bmatrix} 1 \\ i \end{bmatrix}, & |R\rangle &= \frac{1}{\sqrt{2}} \begin{bmatrix} 1 \\ -i \end{bmatrix}.
 \end{aligned} \tag{A1}$$

Under this convention, quarter-wave and half-wave plates are defined as:

$$Q(\theta) = R_y(2\theta)R_z(\pi/2)R_y(-2\theta) \tag{A2}$$

$$H(\theta) = R_y(2\theta)R_z(\pi)R_y(-2\theta), \tag{A3}$$

where

$$R_k(\theta) = \exp\left[-i\frac{\theta}{2}\sigma_k\right] = \cos\frac{\theta}{2}I - i\sin\frac{\theta}{2}\sigma_k. \tag{A4}$$

Similarly, the fixed Faraday rotators are expressed as:

$$F_{\pm} = R_y(\pm\pi/2). \tag{A5}$$

2. Gadget derivation

Having established these definitions, we explicitly show the simplification used in the derivation of the reciprocal gadget in the main text:

$$\begin{aligned}
 H\left(\frac{\pi}{8}\right)F_- &= R_y\left(\frac{\pi}{4}\right)R_z(\pi)R_y\left(-\frac{\pi}{4}\right)R_y\left(-\frac{\pi}{2}\right) \\
 &= R_z(\pi)R_y\left(-\frac{\pi}{4}\right)R_y\left(-\frac{\pi}{4}\right)R_y\left(-\frac{\pi}{2}\right) \\
 &= R_z(\pi)R_y(-\pi) \\
 &= (-iZ)(iY) \\
 &= -iX,
 \end{aligned} \tag{A6}$$

where the first step used:

$$R_y(\theta)R_z(\pi) = R_z(\pi)R_y(-\theta). \tag{A7}$$

The other three simplifications follow using the same steps.

3. Universality of the reciprocal gadget

In this section we will give a proof that the reciprocal gadget presented in the main text is capable of implementing any $U \in \text{SU}(2)$. We first recall the construction of this gadget:

$$\begin{aligned} G_R &= Q(\theta)H(\phi)G_x(\psi)H(-\phi)Q(-\theta) \\ &= Q(\theta)H(\phi)R_x(\psi)H(-\phi)Q(-\theta). \end{aligned} \quad (\text{A8})$$

In [18] it was shown that a combination of one half-wave and quarter-wave plate implements a two-parameter subset of $\text{SU}(2)$ parameterized as:

$$Q(\theta)H(\phi) = R_y(\alpha)R_z(\pi/2)R_y(\beta). \quad (\text{A9})$$

This subset can be equivalently expressed as:

$$R_y(\gamma)R_z(\delta)R_x(\pi/2) \iff R_y(\alpha)R_z(\pi/2)R_y(\beta). \quad (\text{A10})$$

Given a two-waveplate gadget with the above parameterisation, the description in the backwards propagation direction is:

$$H(-\phi)Q(-\theta) = R_x(-\pi/2)R_z(\delta)R_y(\gamma). \quad (\text{A11})$$

Substituting in these parameterisations in (A8) we find:

$$\begin{aligned} G_R &= R_y(\gamma)R_z(\delta)R_x(\pi/2)R_x(\psi)R_x(-\pi/2)R_z(\delta)R_y(\gamma) \\ &= R_y(\gamma)R_z(\delta)R_x(\psi)R_z(\delta)R_y(\gamma). \end{aligned} \quad (\text{A12})$$

We now multiply this expression from the left by $R_x(\pi)$ and use the trivial relation $R_x(\pi)R_x(-\pi) = \mathbb{1}$:

$$\begin{aligned} R_x(\pi)G_R &= R_x(\pi)R_y(\gamma)R_x(-\pi)R_x(\pi)R_z(\delta)R_x(\psi)R_z(\delta)R_y(\gamma) \\ &= R_x(\pi)R_y(\gamma)R_x(-\pi)R_x(\pi)R_z(\delta)R_x(-\pi)R_x(\psi + \pi)R_z(\delta)R_y(\gamma) \\ &= R_y(-\gamma)R_z(-\delta)R_x(\psi + \pi)R_z(\delta)R_y(\gamma) \\ &= R_y(-\gamma)R_z(-\delta)R_x(\psi')R_z(\delta)R_y(\gamma), \end{aligned} \quad (\text{A13})$$

where $\psi' = \psi + \pi$ and we made use of the identities:

$$R_x(\pi)R_y(\gamma)R_x(-\pi) = R_y(-\gamma) \quad (\text{A14})$$

$$R_x(\pi)R_z(\delta)R_x(-\pi) = R_z(-\delta), \quad (\text{A15})$$

in the last step. To show that (A13) is universal it suffices to show that it can apply a phase $\lambda/2$ to an arbitrary state $|u\rangle$:

$$R_x(\pi)G_R |u\rangle = U |u\rangle = e^{i\lambda/2} |u\rangle. \quad (\text{A16})$$

To this end, we choose ψ' , δ and γ such that $R_x(\psi')R_z(\delta)R_y(\gamma)$ maps $|u\rangle$ to $|-\rangle$ times some phase ϕ :

$$R_x(\psi')R_z(\delta)R_y(\gamma) |u\rangle = e^{i\phi} |-\rangle = e^{i(\psi'+\mu)/2} |-\rangle, \quad (\text{A17})$$

where $\mu = \phi - \psi'$. This is always possible since $R_x(\psi')R_z(\delta)R_y(\gamma)$ is a Tait-Bryan rotation. It's evident that the mapping $|v\rangle \rightarrow e^{i\mu/2} |-\rangle$ has to be done by $R_z(\delta)R_y(\gamma)$, since $|-\rangle$ is an eigenstate of $R_x(\psi')$:

$$\begin{aligned} R_z(\delta)R_y(\gamma) |u\rangle &= e^{i\mu/2} |-\rangle \\ R_x(\psi') |-\rangle &= e^{i\psi'/2} |-\rangle. \end{aligned} \quad (\text{A18})$$

We therefore have:

$$\begin{aligned} R_x(\pi)G_R |u\rangle &= R_y(-\gamma)R_z(-\delta)R_x(\psi')R_z(\delta)R_y(\gamma) |u\rangle \\ &= R_y(-\gamma)R_z(-\delta)e^{i(\psi'+\mu)/2} |-\rangle \\ &= e^{i\psi'/2} |u\rangle. \end{aligned} \quad (\text{A19})$$

There is hence always a G_R such that:

$$R_x(\pi)G_R = U, \quad (\text{A20})$$

for any $U \in \text{SU}(2)$, and choosing $U = R_x(\pi)V$ for some $V \in \text{SU}(2)$ shows that that G_R is universal.

4. Waveplate angle calculation

In this section we give an explicit method for determining the waveplate angles α , θ and ϕ in the reciprocal gadget given an arbitrary unitary $U \in \text{SU}(2)$:

$$G_R = Q(\theta)H(\phi)H\left(\frac{\pi}{8}\right)F_-Q\left(\frac{\pi}{2}\right)H(\alpha)Q\left(\frac{\pi}{2}\right)F_+H\left(\frac{\pi}{8}\right)H(-\phi)Q(-\theta) = U. \quad (\text{A21})$$

A python implementation of the algorithm can be found in the online repository [25]. The method essentially consists of going through the proof presented in the previous section backwards. First, define a new unitary V :

$$V = R_x(\pi)U, \quad (\text{A22})$$

then find the eigenphase $-\lambda/2$ and corresponding eigenvector $|v_+\rangle$:

$$V|v_+\rangle = e^{-i\lambda/2}|v_+\rangle. \quad (\text{A23})$$

The angles γ and δ should then be chosen to rotate $|v_+\rangle$ to $|+\rangle$. This can be done by taking:

$$\gamma = \arctan2\left(\text{tr}[Z|v_+\rangle\langle v_+|], \text{tr}[X|v_+\rangle\langle v_+|]\right) \quad (\text{A24})$$

$$\delta = -\arctan2\left(\text{tr}[YR_y(\gamma)|v_+\rangle\langle v_+|R_y^\dagger(\gamma)], \text{tr}[XR_y(\gamma)|v_+\rangle\langle v_+|R_y^\dagger(\gamma)]\right). \quad (\text{A25})$$

The angle ψ is simply given by:

$$\psi = \lambda - \pi. \quad (\text{A26})$$

Next, the rotation angles γ and δ need to be mapped to the corresponding waveplate angles θ and ϕ :

$$Q(\theta)H(\phi) = R_y(\gamma)R_z(\delta)R_x(\pi/2). \quad (\text{A27})$$

To find these waveplate angles, first construct the state:

$$|L'\rangle = R_x(-\pi/2)R_z(-\delta)R_y(-\gamma)|L\rangle, \quad (\text{A28})$$

where:

$$R_x(-\pi/2)R_z(-\delta)R_y(-\gamma) = (Q(\theta)H(\phi))^{-1}. \quad (\text{A29})$$

The quarter-wave plate angle for the order $H(\phi')Q(\theta') = \pm R_y(\gamma)R_z(\delta)R_x(\pi/2)$ can then be found as:

$$\theta' = \frac{1}{2}\arctan2\left(\text{tr}[X|L'\rangle\langle L'|], \text{tr}[Z|L'\rangle\langle L'|]\right) + \frac{\pi}{4}. \quad (\text{A30})$$

To find the half-wave plate angle, construct the state:

$$|H'\rangle = Q(\theta')R_x(-\pi/2)R_z(-\delta)R_y(-\gamma)|H\rangle. \quad (\text{A31})$$

The angle ϕ' is then given as:

$$\phi' = \frac{1}{4}\arctan2\left(\text{tr}[X|H'\rangle\langle H'|], \text{tr}[Z|H'\rangle\langle H'|]\right). \quad (\text{A32})$$

Note that the ambiguity in the overall sign of the unitary doesn't matter due to palindromic order of the total gadget, since $\pm H(\phi')Q(\theta') = \pm ZQ(-\theta')H(-\phi')Z$, and any minus signs cancel. The angles for the order $Q(\theta)H(\phi)$ are found using the waveplate permutation rule:

$$H(\alpha)Q(\beta) = Q(2\alpha - \beta)H(\alpha), \quad (\text{A33})$$

and hence:

$$\phi = \phi' \quad (\text{A34})$$

$$\theta = 2\phi - \theta'. \quad (\text{A35})$$

The last angle, the one of the middle half-wave plate, can be calculated directly from ψ :

$$\alpha = \psi/4 + \pi/2. \quad (\text{A36})$$

Using the waveplate reduction rules [18]:

$$Q(a)H(b)H(c) = Q(a + \pi/2)H(a - b + c - \pi/2) \quad (\text{A37})$$

$$H(a)H(b)Q(c) = H(a - b + c - \pi/2)Q(c + \pi/2), \quad (\text{A38})$$

the gadget can be simplified, removing two waveplates:

$$G_R = Q(\theta_1)H(\phi_1)F_-Q\left(\frac{\pi}{2}\right)H(\alpha)Q\left(\frac{\pi}{2}\right)F_+H(\phi_2)Q(\theta_2) = U, \quad (\text{A39})$$

with:

$$\theta_1 = \theta + \pi/2 \quad (\text{A40})$$

$$\phi_1 = \theta - \phi + \pi/8 - \pi/2 \quad (\text{A41})$$

$$\theta_2 = -\theta + \pi/2 \quad (\text{A42})$$

$$\phi_2 = \pi/8 + \phi - \theta - \pi/2. \quad (\text{A43})$$

5. Definitions of $G^{[i]}$, $G^{\{i\}}$

The commuting and anti-commuting subsets \mathcal{G}_+ , \mathcal{G}_- of

$$\mathcal{G} = \left\{ \mathbb{1}, X, Y, Z, \frac{X+Y}{\sqrt{2}}, \frac{X-Y}{\sqrt{2}}, \frac{X+Z}{\sqrt{2}}, \frac{X-Z}{\sqrt{2}}, \frac{Y+Z}{\sqrt{2}}, \frac{Y-Z}{\sqrt{2}} \right\} \quad (\text{A44})$$

are

$$\begin{aligned} \mathcal{G}_+ &= \{U_i, V_j \in \mathcal{G} \mid [U_i, V_j] = 0\} \\ &= \{U_i, V_j \in \mathcal{G} \mid i = 0 \vee i = j \vee j = 0\} \end{aligned} \quad (\text{A45})$$

and

$$\begin{aligned} \mathcal{G}_- &= \{U_i, V_j \in \mathcal{G} \mid \{U_i, V_j\} = 0\} \\ &= \{U_i, V_j \in \mathcal{G} \mid i = 1, j \in \{2, 3, 8, 9\} \vee \\ &\quad i = 2, j \in \{1, 3, 6, 7\} \vee \\ &\quad i = 3, j \in \{1, 2, 4, 5\} \vee \\ &\quad i = 4, j \in \{3, 5\} \vee \\ &\quad i = 5, j \in \{3, 4\} \vee \\ &\quad i = 6, j \in \{2, 7\} \vee \\ &\quad i = 7, j \in \{2, 6\} \vee \\ &\quad i = 8, j \in \{1, 9\} \vee \\ &\quad i = 9, j \in \{1, 8\}\}. \end{aligned} \quad (\text{A46})$$

6. Supplementary data

In this section we present alternative visualisations of the data presented in the main text, as well as some supplementary data used to generate the main result.

Fig. 5 shows the expectation values for each pair of unitaries in the witness averaged over all runs.

Fig. 6 shows the heralding efficiency in the $|\pm\rangle$ ports of the control qubit. Since the total photon number should be conserved, a linear fit to this data gives the relative detection efficiencies in the two ports. This value was in turn

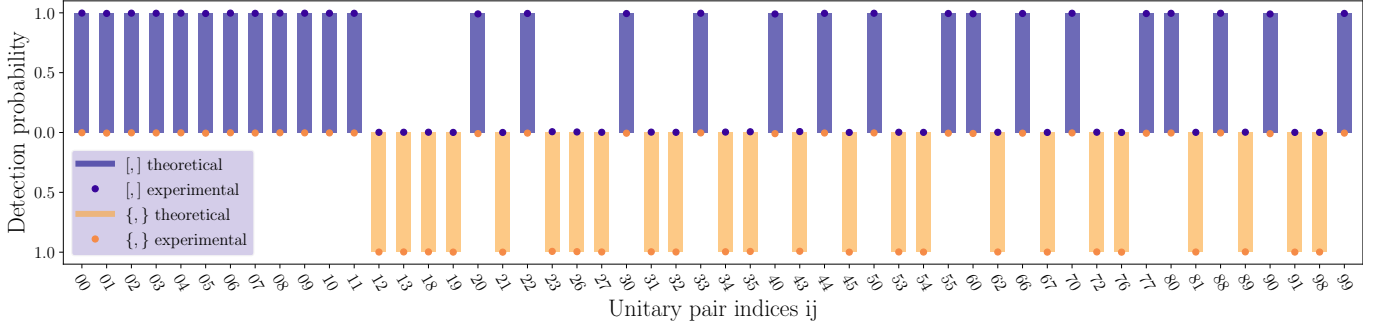


Figure 5. Average winning probabilities. The figure shows the relative probability of a photon to be detected in the commutator and anti-commutator ports of the quantum SWITCH, for every pair of (U, V) in the sets $G^{[,]}$ and $G^{\{, \}}$. The theoretical probabilities $p \in \{0, 1\}$ are shown as solid bars, and the experimentally recorded ones, averaged over all six runs, are indicated by the colored dots. The indices (i, j) on the x-axis specify the pair of unitary operators $(U, V) = (\mathcal{G}_i, \mathcal{G}_j)$.

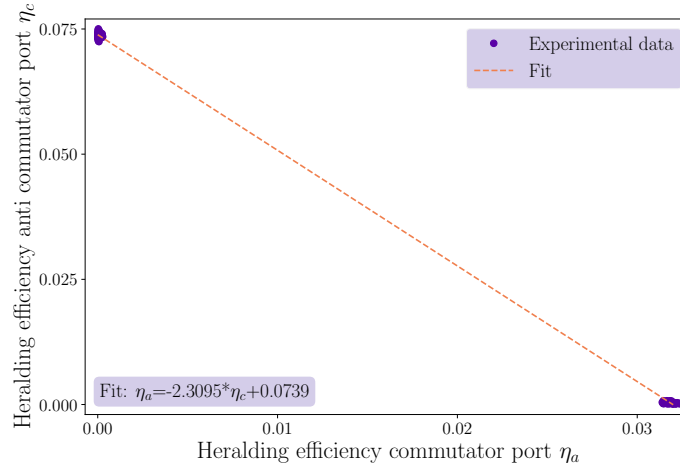


Figure 6. Relative heralding efficiencies. Imbalanced detection efficiencies, as well as loss, between the two output modes of the quantum SWITCH may influence the calculated winning probabilities. As photons must exit the SWITCH in one of either ports, the observed relative heralding efficiencies of unitaries that commute to various degrees follow a linear slope.

used in the evaluation of the success probabilities.. Fig. 7 shows a histogram of the winning probabilities with bin size of 0.001. This data includes all the settings for the six different runs. It can be seen that in the majority of rounds the winning probability exceeds 0.996.

To verify that the gadgets can faithfully implement any unitary, we implement 100 random unitaries W_i , use quantum state tomography to determine the states $W_i^\delta |\Psi\rangle$ for $|\Psi\rangle \in \{|H\rangle, |+\rangle\}$ and $\delta \in \{\text{fw}, \text{bw}\}$, and calculate the quantum state fidelities to the expected states. We define the gate fidelity as the average over Ψ , and show the resulting fidelities as histograms in Fig. 8. The mean gate fidelity over all gadgets and directions of 0.9970 ± 0.0018 indicates that the gadgets are indeed capable of implementing arbitrary unitaries.

Finally, to check that the gadgets are reciprocal, we use the very same measurements, but now calculate the fidelities between $W_i^{\text{fw}} |\Psi\rangle$ and $W_i^{\text{bw}} |\Psi\rangle$. Similarly to before, we define the gadget reciprocity as average over Ψ , and show the results in Fig. 9. With a mean reciprocity of 0.9972 ± 0.0018 , it can be concluded that unitaries implemented by the gadgets are reciprocal. We would like to point out that all unitaries were implemented independently for each direction, hence the reciprocity is affected by imperfect repeatability of the rotation motors moving the gadgets' waveplates.

Appendix B: Causal witness

To characterise the causal structure of quantum processes one can make use of the process matrix formalism [14], in which a quantum process is represented by a positive semidefinite matrix W . The set of all process matrices that represent a definite causal structure, also called causally separable processes matrices, form a convex subset of all

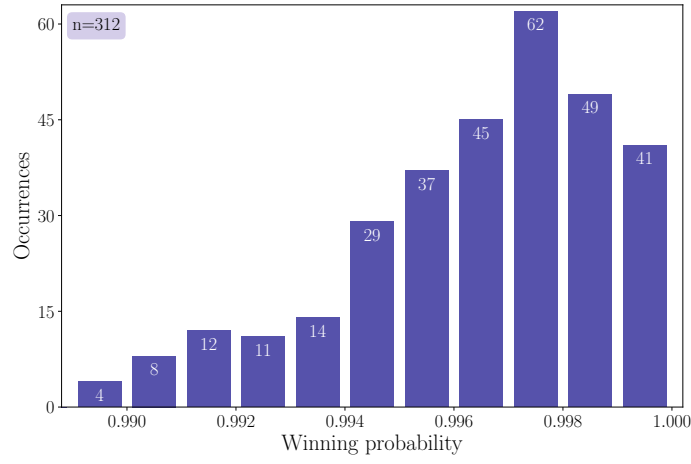


Figure 7. Winning probability histogram (3 runs: $n=312$)

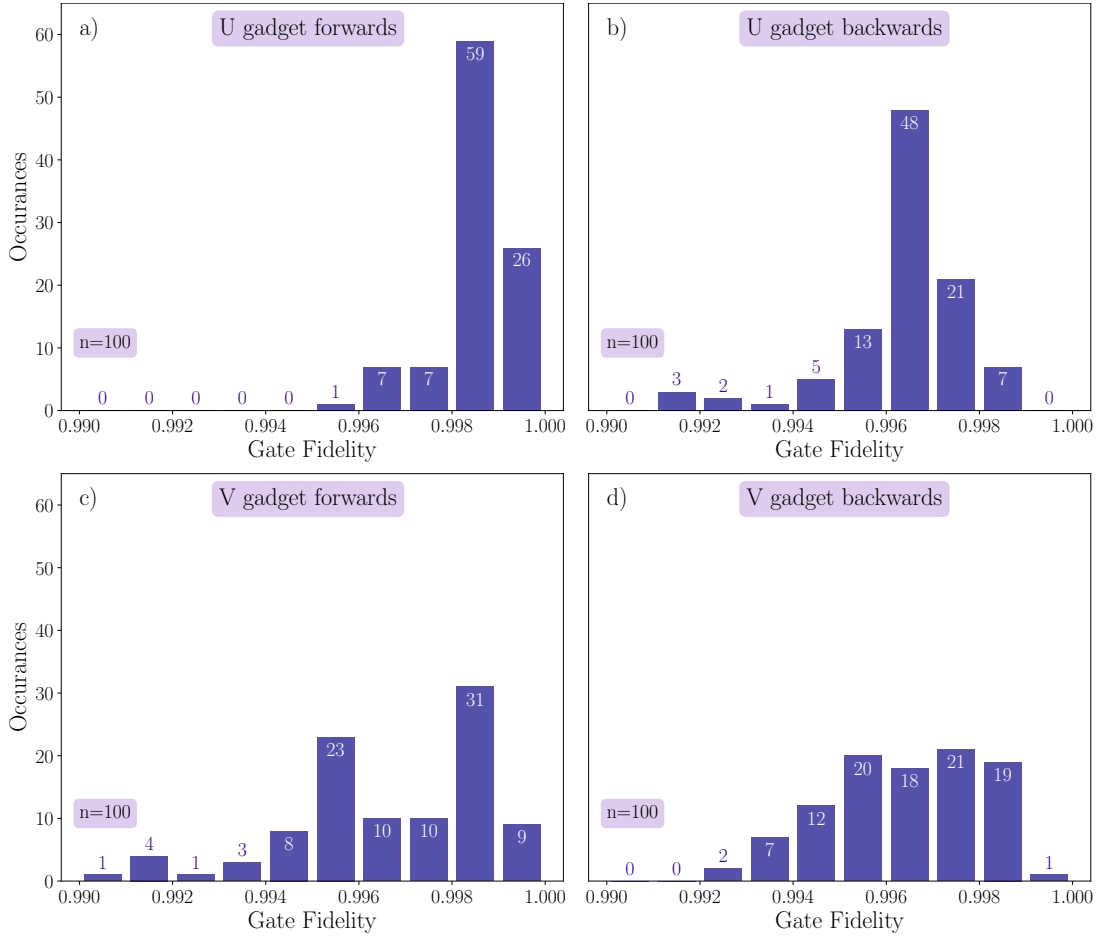


Figure 8. Gate fidelity histograms for both gadgets in forwards and backwards direction. 100 random unitaries W_i were implemented on both gadgets, the states $W_i |H\rangle$ and $W_i |+\rangle$ were measured in both directions independently and the quantum state fidelity between the expected and measured state determined. Depicted are the average fidelities for $|H\rangle$ and $|+\rangle$ for **a)** U_{fw} (Mean fidelity 0.99852 ± 0.00079). **b)** U_{bw} (0.9964 ± 0.0014). **c)** V_{fw} (0.9967 ± 0.0021). **d)** V_{bw} (0.9964 ± 0.0016). The mean fidelity over all gadgets and directions is 0.9970 ± 0.0018 . All uncertainties are standard deviations.

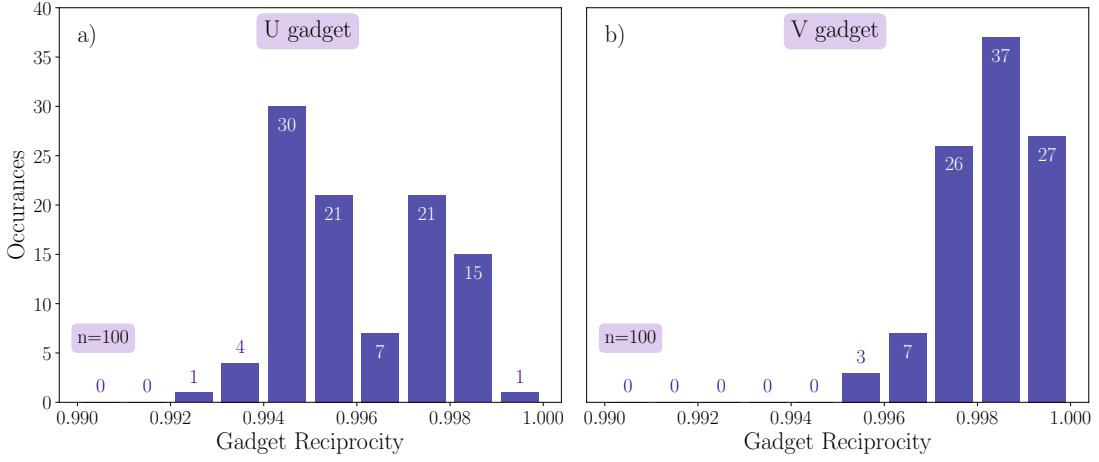


Figure 9. Reciprocity histograms for the two gadgets used in the experiment. 100 random unitaries W_i were implemented on both gadgets, the states $W_i |H\rangle$ and $W_i |+\rangle$ were measured in both directions independently and the quantum state fidelity between the expected and measured state determined. Depicted are the average fidelities for **a)** the U gadget, with mean fidelity of 0.9960 ± 0.0016 and **b)** the V gadget, with a mean fidelity of 0.99834 ± 0.00099 . The mean fidelity for both gadgets is 0.9972 ± 0.0018 . All uncertainties are standard deviations.

process matrices. Consequently, it is always possible to find a hyperplane separating any causally indefinite process matrix from the set of causally separable ones [15]. This in turn implies the existence of a witness operator \mathcal{S} , that can be used to certify the indefinite causal structure of a process. Such a witness has previously been used experimentally to validate the casual non-separability of the quantum SWITCH [7]. Here, we adapt a version of the witness from [15], which is inspired by the task presented in Ref. [3]. Making use of the Choi-Jamiołkowski isomorphism, which allows us to represent linear maps and quantum channels as matrices, the witness can be defined in terms of the operators:

$$G_{\pm}^{i,j} = |U_i\rangle\langle U_i| \otimes |V_j\rangle\langle V_j| \otimes |\pm\rangle\langle \pm|_C, \quad (\text{B1})$$

with:

$$U_i, V_j \in \mathcal{G} = \left\{ \mathbb{1}, X, Y, Z, \frac{X \pm Y}{\sqrt{2}}, \frac{X \pm Z}{\sqrt{2}}, \frac{Y \pm Z}{\sqrt{2}} \right\}. \quad (\text{B2})$$

We then define

$$\mathcal{G}_+ := \left\{ (U_i, V_j) \mid U_i, V_j \in \mathcal{G}, U_i U_j = V_j U_i \right\} \quad (\text{B3})$$

$$\mathcal{G}_- := \left\{ (U_i, V_j) \mid U_i, V_j \in \mathcal{G}, U_i V_j = -V_j U_i \right\} \quad (\text{B4})$$

The witness itself is given by:

$$\mathcal{S} = \frac{1}{N} \sum_{i,j} q_{ij}^{[,]} G_+^{i,j} + q_{ij}^{\{, \}} G_-^{i,j}, \quad (\text{B5})$$

where $q_{ij}^{[,]}$ and $q_{ij}^{\{, \}}$ are weights chosen such that:

$$\begin{aligned} \{(i, j) : [U_i, V_j] = 0\} : q_{ij}^{[,]} &= 1 \\ \{(i, j) : \{U_i, V_j\} = 0\} : q_{ij}^{\{, \}} &= 1, \end{aligned} \quad (\text{B6})$$

and are zero otherwise. Here, similarly to the main text, $N = 52$ is the total number of commuting or anti-commuting pairs of unitaries in \mathcal{G} , and the coefficients above select exactly these subsets. The expectation value of the witness is evaluated as $\langle \mathcal{S} \rangle = \text{tr}[\mathcal{S}W]$, where W is a process matrix [14]. The causal separability bound for the witness described above can be evaluated numerically using the semidefinite programming methods of Ref. [15]. Additionally, the methods from [24] allow us to obtain a computer assisted proof that $\text{tr}[\mathcal{S}W_{\text{sep}}] \leq \frac{90.4}{100}$, for any causally separable process W_{sep} ; the code to certify this value is openly available in an online repository [25]. It can be shown that $\text{tr}[\mathcal{S}W_{\text{SWITCH}}] = 1$, where W_{SWITCH} is the process matrix of the quantum SWITCH.